ELSEVIER

Journal of Organometallic Chemistry 498 (1995) 41–47

Journal of Organometallic Chemistry

Mechanistic studies of the activation and the decomposition of $[Rh_2Cl_2(CO)_4]$ in organometallic chemical vapour deposition

Philippe Serp [a], Roselyne Feurer [b], Roland Morancho [b], Philippe Kalck [a,*], Jean-Claude Daran [c,1], Jacqueline Vaisserman [c]

[a] *Laboratoire de Chimie des Procédés, ENSCT, 118 route de Narbonne, 31077 Toulouse cédex, France*

[b] *Laboratoire de Cristallochimie, Réactivité et Protection des Matériaux (URA-CNRS 445), ENSCT, 118 route de Narbonne, 31077 Toulouse cédex, France*

[c] *Laboratoire de Chimie des Métaux de Transition, 4 Place Jussieu, BP 42, 75252 Paris cédex 05, France*

Received 19 December 1994

Abstract

Various direct and indirect methods have been investigated to show that hydride-rhodium species are generated in the gas phase when vapours of $[Rh_2Cl_2(CO)_4]$ react with dihydrogen for the organometallic chemical vapour deposition of rhodium on silica supports. Mass spectrometric, infrared, and thermogravimetric analyses were carried out to identify the activated species which are produced in the gas phase. Addition of $[AuPPh_3I]$ which is an isolobal analogue of HCl to $[Rh_2Cl_2(CO)_4]$ was examined to simulate the presence of an hydride intermediate and to show the role of dihydrogen. The isolation of $[Rh_2(\mu\text{-}Cl)(\mu\text{-}I)(CO)_3(PPh_3)]$, whose X-ray crystal structure was determined, also supports a primary oxidative addition of H_2 to $[Rh_2Cl_2(CO)_4]$.

Keywords: Rhodium; Organometallic chemical vapour deposition; Catalyst preparation; X-ray structure

1. Introduction

It has recently been shown that highly dispersed supported rhodium catalysts can be conveniently prepared in one step at low temperature by contact of vapours of a precursor with the support in a fluidized bed, producing decomposition to provide nano-scale aggregates of rhodium [1]. The introduction of a partial pressure of dihydrogen into the inert carrier gas led to a large improvement in the purity of the deposit. In particular, in the case of the precursor $[Rh_2Cl_2(CO)_4]$ the use of dihydrogen allowed us to suppress almost completely the incorporation of chlorine in the deposit. Indeed, in the absence of H_2 the atomic ratio Rh/Cl is ca. 1/1 whereas with H_2 the aggregates contain Rh/Cl ca. 98.5/1.5 w/w. As the dynamic sublimation was carried out at 50 °C and the decomposition in the fluidized bed at 100 °C under a constant pressure of 100 Torr (1 Torr = 13.36 Pa), it was of interest to investigate the role of dihydrogen in the mechanism of the organometallic chemical vapour deposition (OMCVD). The reactions which occur in the gas phase have been analyzed. Since the intermediate species have too short a life-time to be directly observed, indirect methods have been used to simulate the role of H_2 and these imply a mechanism involving hydride species.

2. Results and discussion

The process used to prepare supported rhodium catalysts combines the low pressures required for the sublimation of the rhodium precursor with a fluidized bed in order for the deposit to be homogeneously distributed on the surface of the support. By control of the time of deposition, very dispersed aggregates can be obtained. Thus for 0.5% Rh/SiO_2 (w/w), particle sizes of 1.2 nm have been determined, corresponding to a 91% dispersion. As the rhodium complex is present in the

* Corresponding author.

[1] Present adress: Laboratoire de Chimie de Coordination du CNRS, 205 route de Narbonne, 31077 Toulouse cédex, France.

0022-328X/95/$09.50 © 1995 Elsevier Science S.A. All rights reserved
SSDI 0022-328X(95)05462-6

Table 1
Fragmentation of $[Rh_2Cl_2(CO)_4]$ obtained by mass spectrometry with electronic impact at 70 eV

Mass (m/z)	Intensity (%)	Fragment
103	100	$[Rh]^+$
138	7	$[RhCl]^+$
206	9	$[Rh_2]^+$
241	29	$[Rh_2Cl]^+$
276	39	$[Rh_2Cl_2]^+$
304	39	$[Rh_2Cl_2(CO)]^+$
332	37	$[Rh_2Cl_2(CO)_2]^+$
360	45	$[Rh_2Cl_2(CO)_3]^+$
388	63	$[Rh_2Cl_2(CO)_4]^+$

gas phase with a low partial pressure (around 0.06 Torr at 53 °C for a dynamic total pressure of 100 Torr), the mechanisms of the loss of ligands to afford active intermediates in the gas phase may be related to the fragmentation pattern in mass spectrometry.

2.1. Mass spectrometry of $[Rh_2Cl_2(CO)_4]$

Mass spectra were obtained by electronic impact at 70 eV. The various fragments with their masses and relative intensities are presented in Table 1. The species $[Rh_2Cl_2(CO)_4]^+$ loses the four CO ligands step by step to afford $[Rh_2Cl_2]^+$. No phosgene was detected. Then the presence of the $[Rh_2Cl]^+$ and $[RhCl]^+$, as well as $[Rh_2Cl_2]^+$ is indicative of greater stability of the rhodium–chlorine bond compared with the rhodium–carbonyl bond. Moreover, the mass spectra with $[Rh_2]^+$ and $[Rh]^+$ indicate that metallic rhodium can be obtained.

During the OMCVD process, in the absence of any reactive gas, the deposits contain large amounts of chlorine. Indeed, under the experimental conditions (130 °C in the fluidized bed) the Rh/Cl atomic ratio is near to 1/1. X-ray photoelectron spectroscopy analyses of deposits on planar silica substrates formed under the same conditions of temperature and pressure (but in the absence of the fluidized bed) reveal that rhodium is present in the 0 ($E(3d_{5/2}) = 307.4$ eV; $E(3d_{3/2}) =$ 312.0 eV) and III oxidation states ($E(3d_{5/2}) = 308.8$ eV; $E(3d_{3/2}) = 313.6$ eV). Chlorine was detected at $E(2p_{3/2}) = 197.9$ eV and $E(2p_{1/2}) = 199.1$ eV. These values are consistent with terminal rhodium–chlorine bonds rather than bridging rhodium–chlorine bonds [2]. Thus, chlorine could be present as $RhCl_3$ entities as well as metallic rhodium. Pyrolysis products of $[Rh_2Cl_2(CO)_4]$ by Kumar and Puddephat [3] have shown the presence of $RhCl_3$.

In order to determine the reactivity of $[Rh_2Cl_2(CO)_4]$ in the presence of dihydrogen, thermogravimetric analyses have been carried out.

2.2. Thermogravimetric analyses of $[Rh_2Cl_2(CO)_4]$

Under a pure helium atmosphere thermogravimetric analysis shows a single mass loss of 92%, beginning at 75 °C and ending at 150 °C, corresponding mainly to sublimation and vaporization. The mass of the residue is only 8% and shows that almost all of the complex was transferred to the gaseous phase with little decomposition. Moreover, in differential thermal analysis a sharp endothermic peak is detected at 129 °C, consistent with the melting point of the product which compares with the 125 °C value [4]. Under a helium atmosphere containing 20% dihydrogen, the mass loss between 75 and 140 °C is only 60% with a significant residue resulting from decomposition of the complex induced by H_2. On differential thermal analysis, two peaks are observed in addition to the liquidus at 129 °C: one broad endothermic peak which begins at 100 °C, and a sharp peak at 136 °C. The broad peak corresponds to a chemical reaction between $[Rh_2Cl_2(CO)_4]$ and H_2 whereas the sharp peak could be due to the reaction of H_2 with the solid residue since no simultaneous mass loss is observed.

In order to gain more insight into the reaction between the precursor and the reactive gas, infrared measurements were carried out.

2.3. Infrared analyses of $[Rh_2Cl_2(CO)_4]$ in the gas phase

A gas cell was charged with a small amount of $[Rh_2Cl_2(CO)_4]$ and heated slowly from 25 to 200 °C. The initial pressure was either ca. 100 or ca. 760 Torr. In the presence of helium the ν_{CO} bands of vapours of $[Rh_2Cl_2(CO)_4]$ appear at 2108 cm^{-1} (w, sh), 2093 cm^{-1} (vs), 2042 cm^{-1} (vs) with two ^{13}CO satellites at 2084 cm^{-1} (w) and 2010 cm^{-1} (w). Beyond 125 °C the CO bands owing to free carbon monoxide are detected by the two large envelopes centred at 2176 cm^{-1} and 2123 cm^{-1}. As expected, the intensity of the free CO bands increases with simultaneous decrease of the ν_{CO} bands of the complex when the temperature is raised. No trace of phosgene was observed at 1830 cm^{-1}.

When the same experiment was performed under a helium–dihydrogen atmosphere (80:20 vol) the temperature where CO loss by the complex begins is lower (75 °C). In addition to free CO, HCl is detected in the gas phase at 2890 cm^{-1}. Moreover, the rate of the decomposition is significantly, increased with respect to a pure helium atmosphere.

The presence of HCl in the gas phase, as well as a 50 °C decrease in decomposition temperature, is indicative of a direct reaction of H_2 with vapours of $[Rh_2Cl_2(CO)_4]$ to produce a hydride species through an oxidative addi-

tion reaction. A reductive elimination step would produce HCl. This particular reaction has recently been reviewed by Grushin [5]. All our attempts to accumulate IR spectra in order to detect the hydride compounds failed either because they have short life-times or they are in such a low concentration that their absorptions overlap the ν_{CO} bands of the complex. Thus, adding deuterium to the experiment (helium:deuterium ca. 80:20) did not produce a ν_{Rh-D} band in the 1500–1300 cm^{-1} region, even under an atmosphere containing CO in order to stabilize any intermediate Rh–D species. However, DCl was clearly identified by a broad band centred at 2145 cm^{-1}. Finally, the ν_{H2} band expected in the 3000 cm^{-1} region for an η^2-H_2 bonded dihydrogen was not detected. These observations confirm those from mass spectrometry and are consistent with the presence of hydrido-rhodium species of low stability.

2.4. Mass spectrometry in a chemical ionization mode

Direct chemical ionization in mass spectrometry with either CH_4 or NH_3 was used. The use of methane showed unambiguously the quasi-molecular peak $[Rh_2Cl_2(CO)_4H]^+$ at $m/z = 389$. Moreover, a peak at $m/z = 353$ shows that this affords $[Rh_2Cl(CO)_4]^+$ by loss of HCl. No other fragment was detected, particularly mononuclear species. Thus H^+ from CH_5^+ has a high affinity for the precursor $[Rh_2Cl_2(CO)_4]$ and also induces the loss of HCl.

2.5. Attempts to prepare the complex $[Rh_2Cl_2(CO)_4(AuPPh_3)]^+$

The isolobal analogy between H and $AuPPh_3$ has been shown to be a very powerful method for preparing complexes and in some cases has helped to detect the hydride ligands [6–8]. We observed that $AuPPh_3Cl$ does not react with $[Rh_2Cl_2(CO)_4]$ in polar or non-polar solvents even at 70 °C. The reaction of $[Rh_2Cl_2(CO)_4]$ and the ionic species $[AuPPh_3][CF_3SO_3]$ produced $AuPPh_3Cl$ and an unknown triflate-containing complex. However, a clean reaction was obtained by reacting $AuPPh_3I$ in THF between 20 and 40 °C with $[Rh_2Cl_2(CO)_4]$. From the emerald-green solution we isolated the complex $[Rh_2(Cl)(I)(CO)_3(PPh_3)]$ in high yield. An X-ray crystal structure determination was carried out from suitable yellow crystals. Fig. 1 shows a perspective view of the molecule which is in fact $[Rh_2(\mu\text{-}Cl)_{1.5}(\mu\text{-}I)_{0.5}(CO)_3(PPh_3)]$. Table 2 displays selected bond distances and angles. The two rhodium atoms are in a square-planar environment and are bridged by the two halogen atoms. One bridging position is solely occupied by a chlorine atom whereas the other is statistically occupied by chlorine and iodine with an occupancy factor of 0.5 for each. The latter bridging atom is trans to the triphenylphosphine ligand. The distance between the two rhodium atoms is 3.014(2) Å, consistent with most of the distances found in related dirhodium complexes [9]. The X-ray structure of the complex $[Rh_2(\mu\text{-bzta})_2(CO)_3(PPh_3)]$ (where bzta is a benzothiazole-2-thiolato bridging ligand) [9] shows a metal–metal distance of 3.0351(5) Å and each rhodium to also be in a square-planar environment.

The two square planes around each rhodium atom, although slightly distorted towards the idealized geometry, form a dihedral angle of 107.86°. Such a situation is quite usual in the chemistry of the dinuclear bridged rhodium complexes [9]. The value of this angle is directly connected with the distance between the two rhodium atoms. This distance, shorter than the sum of

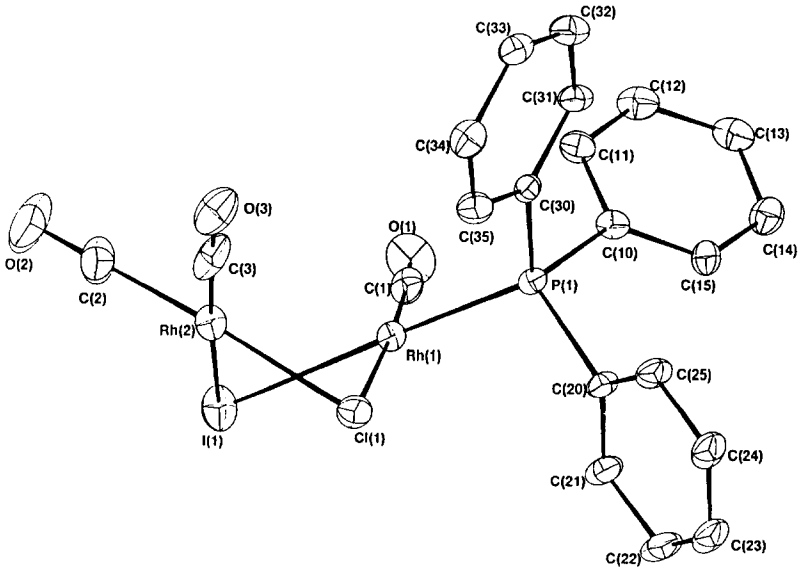

Fig. 1. Molecular representation of $[Rh_2(\mu\text{-}Cl)_{1.5}(\mu\text{-}I)_{0.5}(CO)_3(PPh_3)]$ showing the atom-numbering scheme.

the van der Waals radii, has been interpreted as owing to a weak interaction between the two metal centres [10,11]. The chlorine atom Cl(1) is symmetrically bound, the two Rh–Cl distances being 2.388(4) and 2.375(4) Å. The other bridging atom may be considered as an iodine atom due to its greater number of electrons than chlorine. In this case the Rh(2)X(1) distance is 2.508(3) Å whereas the Rh(1)X(1) distance is 2.651(2) Å. This lengthening is due to the trans influence of the triphenylphosphine. All other distances are in the expected range.

The infrared spectra of $[Rh_2(Cl)(X)(CO)_3(PPh_3)]$ shows three ν_{CO} bands at 2078 cm^{-1} (s), 2018 cm^{-1} (s) and 1989 cm^{-1} (vs) in KBr pellets, and at 2083 cm^{-1} (s), 2031 cm^{-1} (s) and 2019 cm^{-1} (vs) in hexane solutions. There is no detectable equilibrium between this species and $[Rh_2(Cl)(X)(CO)_4]$ and $[Rh_2(Cl)(X)(CO)_2(PPh_3)_2]$. In the ^{31}P NMR spectrum, a single signal is detected at 46.03 ppm (doublet, $^1J_{Rh-P} = 177$ Hz) in $CDCl_3$.

This complex can be considered as resulting from the oxidative addition (OA) of $AuPPh_3I$ to $[Rh_2Cl_2(CO)_4]$ followed by unexpected rearrangement. As shown in Scheme 1, a rhodium(I)–rhodium(III) complex is formed

Table 2
Interatomic distances (Å) and bond angles (deg.) of the complex $[Rh_2(\mu\text{-}Cl)_{1.5}(\mu\text{-}I)_{0.5}(CO)_3(PPh_3)]$

Rh(1)–Rh(2)	3.014(2)	Rh(1)–P(1)	2.248(3)
Rh(1)–Cl(1)	2.388(4)	Rh(1)–C(1)	1.81(2)
Rh(1)–X(1)	2.651(2)	Rh(2)–Cl(1)	2.375(4)
Rh(2)–C(2)	1.85(2)	Rh(2)–C(3)	1.80(2)
Rh(2)–X(1)	2.508(3)	P(1)–C(10)	1.82(1)
P(1)–C(20)	1.84(1)	P(1)–C(30)	1.83(1)
O(1)–C(1)	1.13(2)	O(2)–C(2)	1.12(2)
O(3)–C(3)	1.16(2)	C(10)–C(11)	1.39(2)
C(10)–C(15)	1.37(2)	C(11)–C(12)	1.38(2)
C(12)–C(13)	1.38(2)	C(13)–C(14)	1.44(2)
C(14)–C(15)	1.38(2)	C(20)–C(21)	1.40(2)
C(20)–C(25)	1.35(2)	C(21)–C(22)	1.41(2)
C(22)–C(23)	1.36(2)	C(23)–C(24)	1.34(2)
C(24)–C(25)	1.38(2)	C(30)–C(31)	1.38(2)
C(30)–C(35)	1.38(2)	C(31)–C(32)	1.40(2)
C(32)–C(33)	1.33(2)	C(33)–C(34)	1.37(2)
C(34)–C(35)	1.38(2)		
P(1)–Rh(1)–Rh(2)	123.5(1)	Cl(1)–Rh(1)–Rh(2)	50.56(9)
Cl(1)–Rh(1)–P(1)	93.2(1)	C(1)–Rh(1)–Rh(2)	125.5(4)
C(1)–Rh(1)–P(1)	93.4(5)	X(1)–Rh(1)–P(1)	174.3(1)
X(1)–Rh(1)–Cl(1)	81.2(1)	X(1)–Rh(1)–O(1)	90.2(3)
X(1)–Rh(1)–C(1)	92.2(5)	C(1)–Rh(1)–Cl(1)	173.3(5)
Cl(1)–Rh(2)–Rh(1)	50.94(9)	C(2)–Rh(2)–Rh(1)	127.2(6)
C(2)–Rh(2)–Cl(1)	175.6(5)	C(3)–Rh(2)–Rh(1)	119.7(5)
C(3)–Rh(2)–Cl(1)	94.0(5)	C(3)–Rh(2)–C(2)	90.3(7)
X(1)–Rh(2)–Rh(1)	56.49(6)	X(1)–Rh(2)–Cl(1)	84.5(1)
X(1)–Rh(2)–C(2)	91.3(6)	X(1)–Rh(2)–C(3)	175.9(6)
C(10)–P(1)–Rh(1)	118.2(4)	C(20)–P(1)–Rh(1)	110.6(4)
C(20)–P(1)–C(10)	104.9(6)	C(30)–P(1)–Rh(1)	114.9(4)
C(30)–P(1)–C(10)	102.9(6)	C(30)–P(1)–C(20)	104.0(6)
Rh(2)–Cl(1)–Rh(1)	78.5(1)	Rh(1)–X(1)–Rh(2)	71.43(7)
O(1)–C(1)–Rh(1)	174.7(14)	O(2)–C(2)–Rh(2)	177.9(21)
O(3)–C(3)–Rh(2)	176.1(17)	C(11)–C(10)–P(1)	119.0(10)
C(15)–C(10)–P(1)	121.6(10)	C(15)–C(10)–C(11)	119.3(12)
C(12)–C(11)–C(10)	119.6(13)	C(13)–C(12)–C(11)	122.9(14)
C(14)–C(13)–C(12)	117.2(13)	C(15)–C(14)–C(13)	118.8(13)
C(14)–C(15)–C(10)	122.2(13)	C(21)–C(20)–P(1)	115.2(11)
C(25)–C(20)–P(1)	122.9(10)	C(25)–C(20)–C(21)	121.8(12)
C(22)–C(21)–C(20)	116.2(15)	C(23)–C(22)–C(21)	120.9(15)
C(24)–C(23)–C(22)	120.6(14)	C(25)–C(24)–C(23)	120.7(15)
C(24)–C(25)–C(20)	119.7(13)	C(31)–C(30)–P(1)	122.1(10)
C(35)–C(30)–P(1)	119.6(9)	C(35)–C(30)–C(31)	118.3(12)
C(32)–C(31)–C(30)	119.9(13)	C(33)–C(32)–C(31)	120.8(13)
C(34)–C(33)–C(32)	120.0(13)	C(35)–C(34)–C(33)	120.2(14)
C(34)–C(35)–C(30)	120.8(13)		

in a first step. Such mixed species have been already described. For example, Tolman et al. have shown by ^{31}P and ^{1}H NMR spectroscopy that hydrogenation of $[Rh_2(\mu\text{-}Cl)_2(P(C_6H_4Me)_3)_4]$ gives $[(H)_2(P(C_6H_4Me)_3)_2Rh(\mu\text{-}Cl)_2Rh(P(C_6H_4Me)_3)_2]$ [12]. Poilblanc et al. isolated $[(I)(COCH_3)(PMe_2Ph)Rh(\mu\text{-}S\text{-}Bu^t)_2Rh(CO)(PMe_2Ph)]$ from the OA of CH_3I to $[Rh_2(\mu\text{-}S\text{-}Bu^t)_2(CO)_2(PMe_2Ph)_2]$ [13]. In addition Muetterties et al. published the X-ray structure of $[H_4Rh_2\{P(NMe_2)_3\}_4]$ from the OA of dihydrogen on $[Rh_2(\mu\text{-}H)_2\{P(NMe_2)_3\}_4]$ [14].

Chlorine–iodine exchange at rhodium (III) occurs between the terminal and the bridging positions to produce compound B. Then this may lose CO and bond to triphenylphosphine producing species C. Reductive elimination of AuCl gives rise to $[Rh_2(\mu\text{-}Cl)(\mu\text{-}I)(CO)_3(PPh_3)]$ which has been isolated.

2.6. The nature of the rhodium species in the gas phase

The structures of $[(CO)_2Rh(\mu\text{-}Cl)_2Rh(AuPPh_3)(I)(CO)_2]$ (A) and $[(CO)_2Rh(\mu\text{-}Cl)_2Rh(H)(I)(CO)_2]$ (B) may be considered to be equivalent as H and $AuPPh_3$ are isolobal. This latter complex becomes $[(CO)_2Rh(\mu\text{-}Cl)_2Rh(Cl)(H)(CO)_2]$ just by replacement of iodine with chlorine. Moreover, as the exchange between terminal and bridging atoms seems to be a relatively facile phenomenon, we can consider complex A to in fact be a form of $[(CO)_2Rh(\mu\text{-}Cl)(\mu\text{-}H)Rh(Cl)(H)(CO)_2]$. By reductive elimination this complex can lose HCl as observed in the gas phase by infrared and mass spectrometry. This last complex results from the OA of dihydrogen to $[Rh_2(\mu\text{-}Cl)_2(CO)_4]$ followed by the exchange of a terminal H with a bridging Cl. A second oxidative addition of H_2 and reductive elimination of HCl would generate the species $[Rh_2(\mu\text{-}H)_2(CO)_4]$. Dihydrido-bridged dirhodium complexes have already been described. Muetterties has reported the structure of $[Rh_2(\mu\text{-}H)_2(P(O\text{–}Pr^i)_3)_4]$, which is quite similar to the tetracarbonyl species proposed here [15]. In fact other hydrido-rhodium species such as $[Rh(H)(CO)_2]$ and $[Rh_3(H)_3(CO)_6]$, can also be considered.

In the OMCVD experiments where dihydrogen was omitted, the incorporation of chlorine into the deposit approached one chlorine atom per rhodium atom. Under our experimental conditions the hydroxyl groups at the silica surface do not react with the vapours of $[Rh_2(\mu\text{-}Cl)_2(CO)_4]$ to produce hydrochloric acid, although such a process has been described for hydroxylated alumina surfaces [16,17]. In addition, when dihydrogen is introduced into the reactor at 130 °C after the deposit has been formed, no significant removal of chlorine occurs. If $[Rh_2(\mu\text{-}Cl)_2(CO)_4]$ is adsorbed from the gas phase at 50 °C on the support under the same conditions of gas flow than previously, and if dihydrogen is then introduced into the carrier gas at 130 °C, some chlorine can be removed. Generally Rh/Cl is then ca. 3/1. Hence, since dihydrogen in the gas phase containing $[Rh_2(\mu\text{-}Cl)_2(CO)_4]$ allows not only a lower deposition temperature but also the incorporation of very low amounts of chlorine (1.5%) in the deposit, it is reasonable to conclude that hydrido-rhodium species, having a short lifetime, are present in the gas phase.

The intimate mechanism by which these activated species lead to the anchoring of rhodium on the support surface is under investigation.

3. Experimental

3.1. Mass spectrometry

Mass spectra were obtained on a NERMAG R10-10 spectrometer, either in the electronic impact mode at 70 eV or in the chemical ionization mode using methane.

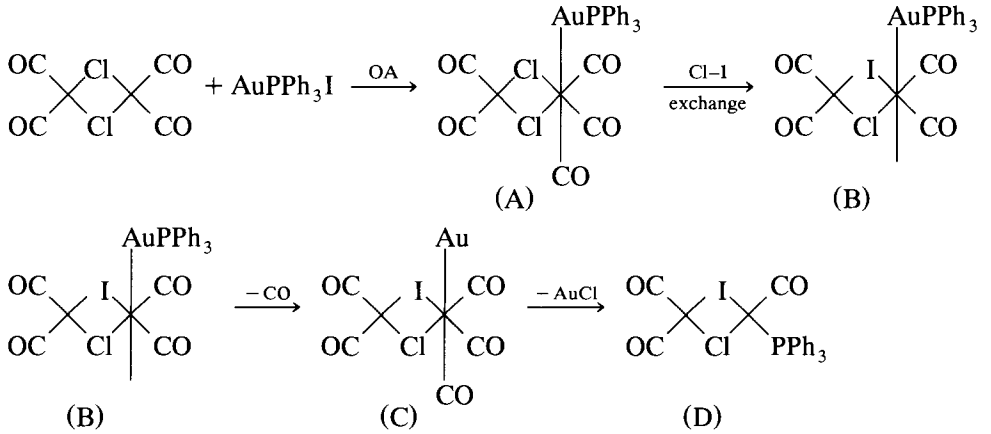

Scheme 1. Proposed mechanisms for the formation of compound D by oxidative addition of $AuPPh_3I$ to $[Rh_2(\mu\text{-}Cl)_2(CO)_4]$. Rhodium atoms have been omitted for clarity.

Table 3
Thermoanalytical study conditions

Conditions	DTA	TGA
Ramps of temperature	5°C min^{-1} from 20 to 50°C	
	1°C min^{-1} from 50 to 150°C	
Min. temperature	20°C	
Max. temperature	150°C	
Nature of the gas	He and He/H_2 (80/20)	

3.2. Infrared spectroscopy

Infrared spectra were obtained on a Perkin–Elmer FTIR 1710 spectrometer. The rhodium complex (10 mg) was placed in a dioxygen-free gas cell heated between 20 and 200 °C, the temperature of the cell being controlled by a K-type thermocouple.

3.3. Thermoanalytical studies (DTA / TGA)

Thermoanalytical studies were conducted under a helium or helium/dihydrogen atmosphere in the dynamic mode (Table 3). DTA analyses were carried out on a Setaram 80 thermobalance and TGA analyses with a B60 DAM Setaram thermobalance (program PRT 3000 by Setaram).

3.4. Synthesis of $[Rh_2(\mu\text{-}Cl)_{1.5}(\mu\text{-}I)_{0.5}(CO)_3(PPh_3)]$

A solution of $[Rh_2(\mu\text{-}Cl)_2(CO)_4]$ (120 mg, 0.308 mmol) was added slowly to a stirred solution of $AuPPh_3I$ (180 mg, 0.308 mmol) in anhydrous THF (20 ml) at 40 °C. The initially yellow solution turned emerald green in few minutes with the formation of a grey precipitate of AuCl. After separation using a canula, the solvent was removed under vacuum and the product was extracted with 10 ml of hexane. Crystallisation at −25 °C produced the complex as well-shaped yellow crystals (148 mg, 74%).

IR (KBr, cm^{-1}): ν_{CO} 2078 (s), 2018 (s) and 1989 (vs). $^{31}P\{^1H\}$ NMR ($CDCl_3$, 20 °C): 46.03 ppm (doublet, $^1J_{Rh-P} = 177$ Hz). Anal. Found: C = 37.92%, H = 2.29%, O = 7.29%. $C_{21}H_{15}Cl_{1.5}I_{0.5}O_3P_4Rh$. Calcd.: C = 37.71%, H = 2.24%, O = 7.17%.

3.5. Crystal data

Unit cell dimensions of a selected crystal were obtained from least-squares refinements of the setting angles of 25 well-centred reflections. Two standard reflections were monitored periodically and showed no change during data collection carried out at 21 °C. Crystallographic data and other pertinent information are summarized in Table 4. Corrections were made for Lorentz and polarization effects. Empirical absorption corrections (Difabs) [18] were applied.

Computations were performed using CRYSTALS [19] adapted to a PC. Atomic form factors for neutral C, O, P, Rh, Cl, I and H were taken from Ref. [20]. Anomalous dispersion was taken into account. The structure was solved by direct methods and subsequent Fourier maps (SHELXS-86) [21]. Almost all hydrogen atoms were found on difference maps, others were geometrically located. Their positions were not refined but recalculated after each cycle. They were given an overall isotropic thermal parameter. Non-hydrogen atoms were anisotropically refined. Least-squares refinements with approximations in three blocks to the normal matrix were carried out by minimizing the function $\Sigma w(|F_o| - |F_c|)^2$, where F_o and F_c are the observed and calculated structure factors. The unit weight was used. The model reached convergence with $R = \Sigma(||F_o| - |F_c||)/\Sigma|F_o|$ and $R_w = [\Sigma w(|F_o| - |F_c|)^2/\Sigma w(F_o)^2]^{1/2}$ having values listed in Table 4. The criteria for a satisfactory complete analysis were the ratios of rms shift to standard deviation being less than 0.1 and no significant features appearing in the final difference map.

Table 4
Crystallographic data

Crystal parameters	
Compound	$C_{21}H_{15}PO_3Rh_2Cl_{1.5}I_{0.5}$
F_w	619.4
Crystal system	triclinic
Space group	$P\bar{1}$
a (Å)	8.973(2)
b (Å)	10.502(3)
c (Å)	12.530(2)
α (deg)	104.92(2)
β (deg)	102.56(2)
γ (deg)	92.01(2)
V (Å^3)	1108.3(6)
Z	2
ρ (calcd) (g cm^{-3})	1.86
μ (Mo Kα) (cm^{-1})	23.8
Data collection	
Diffractometer	Enraf-Nonius CAD 4F
Monochromator	Graphite
Radiation	Mo Kα (0.71073)
Scan type	$\omega/2\theta$
Scan range θ (deg)	$0.8 + 0.345\text{tg}\,\theta$
2θ range (deg)	50
Reflection collected	4096
Reflection merged (R_m)	3899 (0.024)
Reflection used ($I > 3\sigma(I)$)	2523
Refinement	
R (%)	5.31
R_w (%)	6.24
Abs. corr.	Difabs
Min./max. correction	0.98/1.0
Weighting scheme	unity
I.s. parameters	264

Table 5
Fractional atomic coordinates of the complex $[Rh_2(\mu\text{-}Cl)_{1.5}(\mu\text{-}I)_{0.5}(CO)_3(PPh_3)]$

Atom	x	y	z	U (eqv)
Rh(1)	−0.1551(1)	0.1579(1)	0.24893(9)	0.0347
Rh(2)	−0.2599(1)	0.2644(1)	0.4649(1)	0.0490
P(1)	−0.0968(4)	0.2852(3)	0.1416(3)	0.0310
Cl(1)	−0.0224(4)	0.3158(4)	0.4224(3)	0.0479
X(1) [a]	−0.2111(3)	0.0274(2)	0.3933(2)	0.0576
O(1)	−0.323(2)	−0.059(1)	0.057(1)	0.0671
O(2)	−0.551(2)	0.181(2)	0.514(2)	0.1004
O(3)	−0.325(1)	0.544(1)	0.526(1)	0.0708
C(1)	−0.258(2)	0.027(1)	0.127(1)	0.0434
C(2)	−0.440(2)	0.214(2)	0.497(2)	0.0685
C(3)	−0.297(2)	0.435(2)	0.506(1)	0.0550
C(10)	−0.147(1)	0.217(1)	−0.012(1)	0.0331
C(11)	−0.297(2)	0.165(1)	−0.066(1)	0.0431
C(12)	−0.336(2)	0.114(1)	−0.183(1)	0.0491
C(13)	−0.231(2)	0.109(2)	−0.249(1)	0.0501
C(14)	−0.076(2)	0.162(2)	−0.192(1)	0.0501
C(15)	−0.040(2)	0.215(1)	−0.076(1)	0.0413
C(20)	−0.111(1)	0.334(1)	0.178(1)	0.0357
C(21)	−0.205(2)	0.231(2)	0.188(1)	0.0475
C(22)	−0.364(2)	0.265(2)	0.211(1)	0.0516
C(23)	−0.422(2)	0.391(2)	0.224(1)	0.0506
C(24)	−0.328(2)	0.485(2)	0.212(1)	0.0495
C(25)	−0.171(1)	0.458(1)	0.189(1)	0.0397
C(30)	−0.182(1)	0.443(1)	0.161(1)	0.0314
C(31)	−0.265(1)	0.482(1)	0.071(1)	0.0397
C(32)	−0.327(2)	0.605(1)	0.090(1)	0.0481
C(33)	−0.310(2)	0.682(1)	0.196(1)	0.0454
C(34)	−0.226(2)	0.645(1)	0.286(1)	0.0489
C(35)	−0.162(2)	0.526(1)	0.269(1)	0.0451

[a] X(1) is 0.50 I + 0.50 Cl.

The two rhodium atoms are bridged by a chlorine atom and by atom X, the position of which is statistically occupied by chlorine and iodine (occupancy factor 0.5 for each atom). The atomic coordinates are given in Table 5 and Table 2 contains the interatomic distances and bond angles.

The view of the molecule was obtained using CAMERON [19]. The ellipsoids represent 30% probability.

Tables of anisotropic temperature factors, coordinates of hydrogen atoms, and important least-squares planes have been deposited with the Cambridge Crystallographic Data Centre. A list of observed and calculated structure factors is available from the authors.

Acknowledgments

Financial support of the European Economic Community (BRITE-EURAM, BREU CT 091) and the Région Midi-Pyrénées is gratefully acknowledged. We thank the Comptoir Lyon-Alemand-Louyot for the generous gift of rhodium trichloride.

References

[1] P. Serp, R. Feurer, R. Morancho and Ph. Kalck, *J. Mol. Catal.*, in press.
[2] J.R. Ebner, D.L. Mc Fadden, D.R. Tyler and R.A. Walton, *Inorg. Chem.*, *15* (1976) 3014.
[3] R. Kumar and R.J. Puddephatt, *Can. J. Chem.*, *69* (1991) 108.
[4] J.A. Mc Cleverty and G. Wilkinson, *Inorg. Synth.*, *8* (1963) 211.
[5] V.V. Grushin, *Acc. Chem. Res.*, *26* (1993) 279.
[6] R. Hoffman, *Angew. Chem. Int. Ed. Engl.*, *21* (1982) 71.
[7] D. Michael, P. Mingos and J. Watson, *Adv. Inorg. Chem.*, *39* (1992) 327.
[8] S.L. Schiavo, G. Bruno, F. Nicolo, P. Piraino and F. Faraone, *Organometallics*, *4* (1985) 2091.
[9] M.A. Ciriano, J.J. Pérez-Torrente, F.J. Lehog and L.A. Oro, *J. Organomet. Chem.*, *455* (1993) 225, and references cited therein.
[10] R.S. Dickson, F. Carnovale and J.B. Peel, *J. Organomet. Chem*, *179* (1979) 115.
[11] J.F. Nixon, R.J. Suffolk, M.J. Taylor, J.G. Norman, Jr., D.E. Hoskins and D.J. Gmur, *Inorg Chem.*, *19* (1980) 810.
[12] C.A. Tolman, P.Z. Meakin, D.L. Linder and J.P. Jesson, *J. Am. Chem. Soc.*, *96* (1974) 2762.
[13] A. Mayanza, J.J. Bonnet, J. Galy, Ph. Kalck and R. Poilblanc, *J. Chem. Res. (M)*, (1980) 2101.
[14] E.B. Meier, R.R. Burch and E.L. Muetterties, *J. Am. Chem. Soc.*, *104* (1982) 2661.
[15] A.J. Sivak and E.L. Muetterties, *J. Am. Chem. Soc.*, *101* (1979) 4878.
[16] W.H. Bowser and W.H. Weinberg, *J. Am. Chem. Soc.*, *103* (1981) 1453.
[17] J.M. Rasat, A. Theolier, D. Commereuc and Y. Chauvin, *J. Organomet. Chem.*, *279* (1985) 1470.
[18] N. Walker and D. Stuart, *Acta Crystallogr.*, *39* (1983) 158.
[19] D.J. Watkin, J.R. Carruthers and P.W. Betteridge, CRYSTALS, An advanced crystallographic program system, Chemical Crystallography Laboratory, University of Oxford, Oxford, UK, 1988.
[20] *International Tables for X-ray Crystallography*, Vol. IV, Kynoch Press, Birmingham, UK, 1974.
[21] G.M. Sheldrick, SHELXS-86, Program for crystal structure solution, University of Göttingen, 1986.